ARL-TR-9090 ● Oct 2020

DEVCOM ARMY RESEARCH LABORATORY

Flash Sintering of Boron Carbide (B_4C)

by Andrew Rosenberger, Ray Brennan, Selva Vennila-Raju, and Aubrey L Fry

NOTICES

Disclaimers

The research reported in this document was performed in connection with contract/instrument W911QX-16-D-0014 with the US Army Research Laboratory. (As of 31 January 2019, the organization is now part of the US Army Combat Capabilities Development Command [formerly RDECOM] and is now called CCDC Army Research Laboratory [ARL].) Selva Vennila-Rajju was sponsored by ARL under Cooperative Agreement No. W911NF-16-2-0050.

Research was sponsored by ARL and was accomplished under Cooperative Agreement Number W911NF-16-2-0008 and W911NF-18-2-0117. The views and conclusions contained in this document are those of the authors and should not be interpreted as representing the official policies, either expressed or implied, of ARL or the US Government.

ARL-TR-9090 ● OCT 2020

Flash Sintering of Boron Carbide (B_4C)

Andrew Rosenberger
Bennett Aerospace

Ray Brennan
Weapons and Materials Research Directorate, CCDC Army Research Laboratory

Selva Vennila-Raju
Oak Ridge Associated Universities

Aubrey L Fry
Pennsylvania State University

REPORT DOCUMENTATION PAGE

Form Approved
OMB No. 0704-0188

1. REPORT DATE *(DD-MM-YYYY)*	2. REPORT TYPE	3. DATES COVERED
October 2020	Technical Report	1 October 2018–31 December 2019

4. TITLE AND SUBTITLE
Flash Sintering of Boron Carbide (B_4C)

5a. CONTRACT NUMBER

5b. GRANT NUMBER

5c. PROGRAM ELEMENT NUMBER

6. AUTHOR(S)
Andrew Rosenberger, Ray Brennan, Selva Vennila-Raju, and Aubrey L Fry

5d. PROJECT NUMBER

5e. TASK NUMBER

5f. WORK UNIT NUMBER

7. PERFORMING ORGANIZATION NAME(S) AND ADDRESS(ES)
CCDC Army Research Laboratory
ATTN: FCDD-RLW-ME
Aberdeen Proving Ground, MD 21005-5066

8. PERFORMING ORGANIZATION REPORT NUMBER
ARL-TR-9090

9. SPONSORING/MONITORING AGENCY NAME(S) AND ADDRESS(ES)

10. SPONSOR/MONITOR'S ACRONYM(S)

11. SPONSOR/MONITOR'S REPORT NUMBER(S)

12. DISTRIBUTION/AVAILABILITY STATEMENT
Approved for public release; distribution is unlimited.

13. SUPPLEMENTARY NOTES
ORCID IDs: Andrew Rosenberger, 0000-0003-3993-4866; Ray Brennan, 0000-0001-5421-4467; Selva Vennila-Raju, 0000-0003-2532-8654; Aubrey Fry, 0000-0001-5571-2337

14. ABSTRACT
Flash sintering of boron carbide (B_4C) with DC and AC currents across a range of field strengths, temperatures, specimen sizes, and electrodes was investigated. Fully dense B_4C was obtained by flash sintering at furnace temperatures as low as 370 °C, but only in a small portion of the specimen volume due to current localization. Application of an isothermal voltage or current ramp at temperatures of 550 or 1100 °C prevented current localization, but the resultant lower power density was insufficient to raise the specimen temperature high enough to obtain fully dense specimens. Scalable densification of B_4C at low furnace temperatures with flash sintering is hypothesized to be possible with a higher current power supply or by thermally isolating the specimen to reduce energy loss.

15. SUBJECT TERMS
ceramics, sintering, energy-coupled to matter, electric field, flash, boron carbide, B_4C

16. SECURITY CLASSIFICATION OF:			17. LIMITATION OF ABSTRACT	18. NUMBER OF PAGES	19a. NAME OF RESPONSIBLE PERSON
a. REPORT	b. ABSTRACT	c. THIS PAGE			Andrew Rosenberger
Unclassified	Unclassified	Unclassified	UU	48	19b. TELEPHONE NUMBER (Include area code) (410) 306-0702

Contents

List of Figures

List of Tables

1. Introduction

Flash sintering is a relatively new technique, first reported in 2010 by researchers at the University of Colorado Boulder. Initial reports found that application of a DC voltage while heating a small dog-bone-shaped yttria-stabilized zirconia (YSZ) specimen caused a sudden decrease in the resistance of the specimen at a critical combination of furnace temperature and applied voltage conditions. This decrease in resistance triggered a rapid increase in current and power from the applied voltage, leading to rapid heating of the specimen and enabling near-full densification at temperatures and times substantially lower than conventional sintering methods.[1]

The technique differs from previous field-enhanced sintering technologies such as spark-plasma sintering (SPS) in several key ways. In terms of the system design, a flash sintering setup applies a high-voltage low-current electric field directly to the specimen in combination with a separate external heating system. SPS uses a high-current low-voltage waveform run directly through the die and sample in a loaded configuration without external heating. SPS typically operates using a kilo-amp-scale pulsed DC current, while flash sintering operates with a benchtop scale DC/AC power supply in the single-amp range.[2–4] SPS is restricted to a cylindrical specimen geometry similar to hot pressing, while flash sintering is theoretically capable of densifying a wider range of specimen geometries. Flash sintering is capable of reaching high density at lower furnace temperatures than SPS, with a substantially lower cost and less complex experimental setup. A visual overview of these system configurations is presented in Fig. 1.

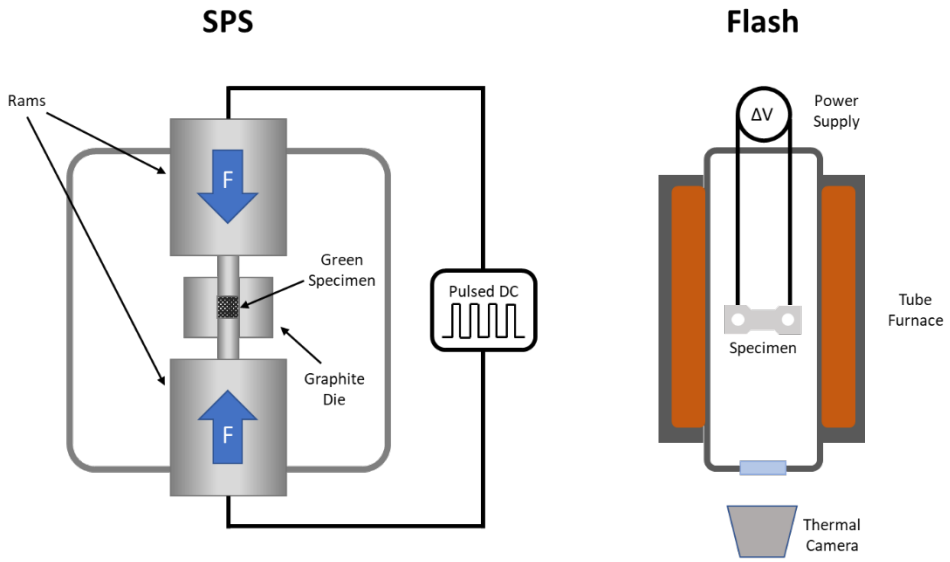

Fig. 1 SPS device[2] (left) compared with (right) a dog-bone-style flash sintering setup[5]

Academic research on flash sintering has primarily focused on investigating the mechanisms behind the flash event and expanding the range of materials that can be sintered. Review papers by Biesuz and Sglavo[6] and Todd[7] provide an excellent overview of these efforts. Thermal runaway from resistive heating, as proposed independently by Todd et al.[8] and Zhang et al.[9] in 2015, has emerged as the generally accepted model for the flash phenomenon. Ceramics are typically electronic insulators where resistivity decreases as temperature increases. Applying a constant voltage with variable current raises the specimen temperature via joule heating and reduces the resistance, further increasing the current. This leads to an increase in the power supplied to the specimen and an additional increase in temperature repeating the cycle. This feedback loop is balanced by thermal losses to the surroundings, which scale with the temperature difference between furnace and specimen. As shown in Fig. 2, the energy gain becomes higher than thermal loss at all temperature differentials at a critical temperature. This triggers the runaway heating "flash" event, which is constrained only by the electrical limits of the power supply.[8]

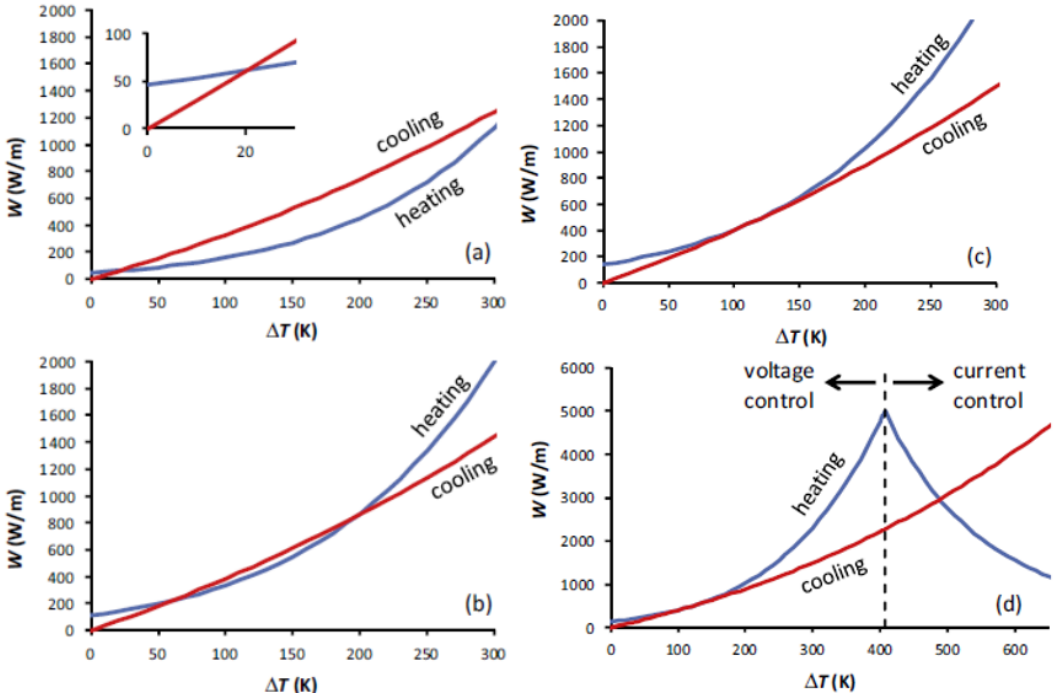

Fig. 2 Data from Todd et al.[8] showing the modelled comparison of joule heating and radiative cooling as a function of excess specimen temperature (ΔT) for YSZ under an electric field of 100 V/cm at different furnace temperatures a) 1250 K, b) 1320 K, c) 1339 K, and d) 1339 K as in (c) but switching to current control at 0.5 A. At the low temperatures in (a) and (b), cooling losses exceed heating gains, resulting in a stable temperature, while at (c) 1320 K, energy input exceeds cooling losses across all values of ΔT, leading to thermal runaway, arrested by the switch to current control (d).

Thermal runaway has successfully modeled flash phenomenon in multiple material systems and configurations, and has been used to explain the observed thermal and sintering behavior. The critical factors influencing the sintering phenomenon are identified as 1) specimen electrical conductivity across temperature and microstructure, 2) electric field and current density applied to the specimen as determined by the power supply and specimen geometry, and 3) thermal loss via conduction, convection, and radiation, which depends mainly on furnace temperature, specimen geometry, and electrode design. Additional effects can come from thermal gradients within the specimen, which can promote hot spot or other nonuniform phenomena.[6] While thermal runaway accounts for the majority of observed flash sintering behavior, additional effects from other proposed mechanisms, such as defect-field interactions and local grain-boundary heating on microstructure and electronic properties, cannot be completely discounted, especially in oxide ceramics where ionic defects and migration can play a role.

Flash sintering has been demonstrated in numerous materials systems, but the vast majority of research has been focused on oxide ceramics (Fig. 3).[3] Some efforts have been made to demonstrate flash sintering in non-oxide ceramics or metals. However, evaluation of these efforts is hindered by confusion of terminology, as several researchers refer to similar techniques, such as SPS with modified die geometries, as "flash sintering". To date, there have been no publications demonstrating flash sintering of Army-relevant non-oxide materials such as boron carbide (B_4C), silicon carbide (SiC), or zirconium diboride using setups other than modified SPS furnaces. Attempts have been made to scale flash-sintering systems beyond the small dog-bone geometries typically used in experiments. The most-common alternate setup geometry consists of a small pellet held in contact between two electrodes by gravity or a dilatometer.[6,10] Different temperature/time/current profiles have been investigated, with findings indicating that AC current can reduce electrode effects and improve control over microstructure.[11–13] Attempts at scale-up are being explored to support industrial production, with a continuous flash-sintering system demonstrated on tile ware by researchers from Lucideon Ltd and University of Colorado Boulder.[14]

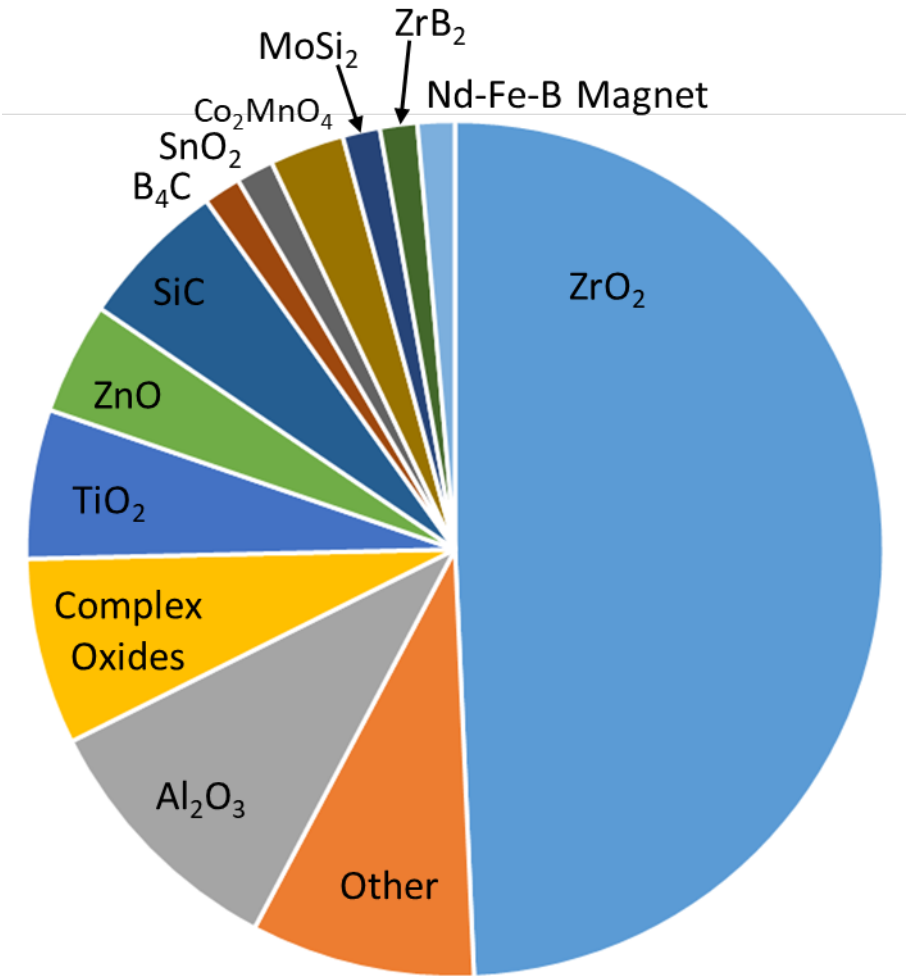

Fig. 3 Proportion of flash sintering papers by material type, 2010–2016[3]

Studies on scaling flash sintering to larger specimens have also investigated cases where specimens form "hot spots" or "channels" of localized high temperatures during flash, which cause nonuniform densification and grain growth. Research by Charalambous et al. found that application of isothermal current ramps helped prevent hot-spot formation in oxides by avoiding the large power spike at the onset of flash.[15] Another study by Trombin et al. on whiteware ceramics, studying the application of different field strengths and operating temperatures, found that uniform densification required limiting the flash event to a "safe" zone of operating parameters.[16]

Aside from the economic benefits of reduced processing time and temperature, the main benefits of flash sintering are its ability to densify materials that are difficult to sinter due to thermal decomposition or reactions and the potential for field-induced defects leading to improved physical or mechanical properties. Densification of traditionally difficult-to-sinter materials such as potassium niobate[17] or bismuth iron oxide[18] with fine microstructures and improved electronic properties has been demonstrated using flash techniques. Additionally, research by Li et al. has found that flash-sintered titania has an abnormally high defect concentration, leading to enhanced room-temperature plasticity in micro-pillar compression tests that exhibit shear banding.[19] These results indicate that flash sintering could be used as a tool to enable processing of new ceramic materials or enhancing material properties beyond what is possible with conventional sintering technologies.

Army interest in flash sintering is driven by the need for enhanced Soldier protection. Flash sintering of current armor ceramics such as B_4C and SiC could enable substantially lower production costs and improved armor properties, and may enable densification of emerging materials such as B_6O. Significant knowledge gaps exist in these areas, with no existing research documenting the response of B_4C to flash sintering in a non-SPS configuration. The goals of the research presented in this report are to determine if flash sintering of B_4C is possible and, if so, to scale the process to produce specimen sizes sufficient for standard mechanical property measurements.

2. Experimental Methods

2.1 Specimen Preparation

All specimens were prepared from HC Starck B_4C powder, Lot 1711/02. The average powder size was 1.9 µm, as measured by laser scattering, and the surface area was 4.44 m^2/g, as measured by Brunauer–Emmett–Teller analysis. Powder was inserted into a cylindrical steel die and pressed at 170 MPa using a Carver uniaxial hydraulic press. Specimen mass was set to produce parts approximately 4.5 mm in height for each die diameter, with 0.2 g powder used for 6-mm-diameter specimens and 1.0 g powder used for 13-mm-diameter specimens. After pressing, pellets were ejected from the die and vacuum-sealed. The pellets were then cold isostatically pressed at 300 MPa for 30 s, removed from the vacuum bag, and placed in a vacuum oven at 80 °C for at least 24 h prior to flash experiments. Specimen density was calculated by measuring the dimensions and mass and by comparing with the theoretical density of B_4C (2.54 g/cm^3). Specimens were typically 65.6 ± 1.6% of theoretical density after cold isostatic pressing.

2.2 Electrode Configurations

A parallel plate electrode configuration using cylindrical specimens (Fig. 4) was used for all experiments. This was selected over the dog-bone-shaped configuration to produce larger, more-scalable specimens. Electrical contact was maintained by placing a weight on the electrodes to press down on the specimens and was verified by visual inspection and resistance measurements prior to initiating the experiments. Three different contact materials were used, including a graphite–ethanol slurry (referred to as graphite paste) painted onto the specimen surfaces, graphite foil, and polished titanium diboride (TiB_2). Three different electrode geometries were used in conjunction with the contact materials. For graphite foil contacts, graphite foil was wrapped around an alumina brick for use as the bottom electrode. The top electrode consisted of either graphite foil wrapped around a 321.2-g pair of alumina bricks placed atop the specimen (Fig. 4b) or a 33.0-g graphite punch in an alumina sleeve placed atop the specimen (Fig. 4c). Graphite paste contacts were used by applying the paste to the specimen top and bottom and then inserting them into the aforementioned graphite foil/alumina brick setup. The TiB_2 electrode configuration consisted of two 1-inch-diameter 44.2-g (top) cylinders of TiB_2 polished to a 1-µm finish. The specimen was placed in between the stacked electrodes (Fig. 4d). Chromel wires were used to connect the electrodes to the power supply.

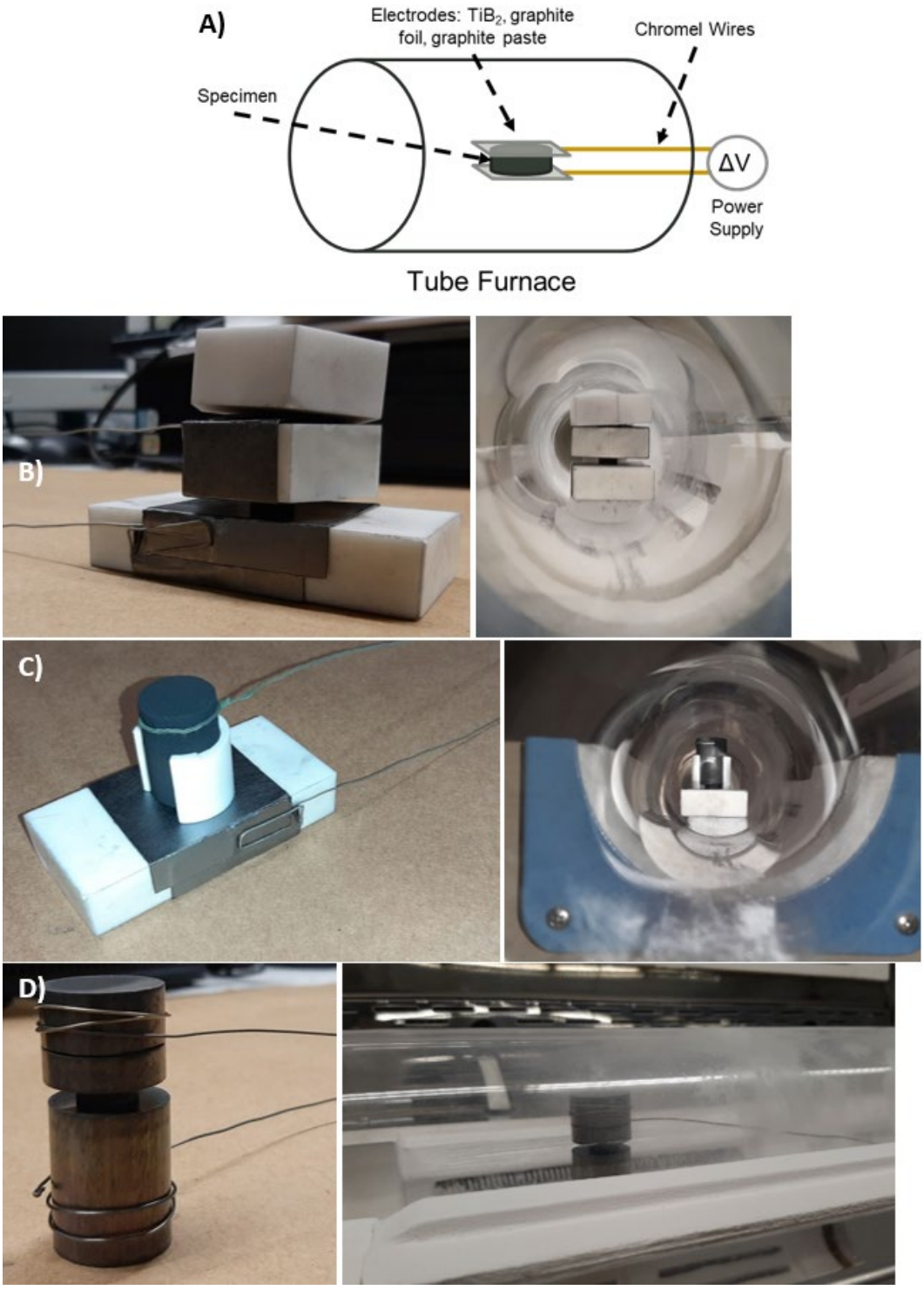

Fig. 4 A) Generic schematic of the flash sintering electrodes, B) photographs of the alumina brick configuration with graphite foil contacts, C) photographs of the graphite punch with graphite foil configuration, and D) photographs of the TiB_2 electrode configuration

2.3 DC Flash Apparatus

Experiments were initially conducted using a DC flash sintering system constructed from an MTI OTF-1200X dual-zone quartz tube furnace and an MPJA Model 9313-PS 125-V/3-A DC power supply. Removable flanges were used to seal the ends of the tube, enabling experiments to be run under atmosphere, low vacuum, or inert gas. A 1-Ω resistor was placed in series with the circuit to provide base resistance. Open circuit resistance of the setup at room temperature was typically measured at 5.5 ± 2.5 Ω (95% confidence limit). Temperature profiles were controlled via set-point programs entered into the built-in temperature controllers. Temperature set point and thermocouple values were recorded with a custom Python script that interfaced with the furnace. The applied voltage was controlled manually, while current and applied voltage were measured and recorded by TracerDAQ, using the sense ports on the power supply. A circuit diagram of the setup is provided in Fig. 5. Electrical measurements from this system were reported without processing to eliminate the effects of the 1-Ω resistor.

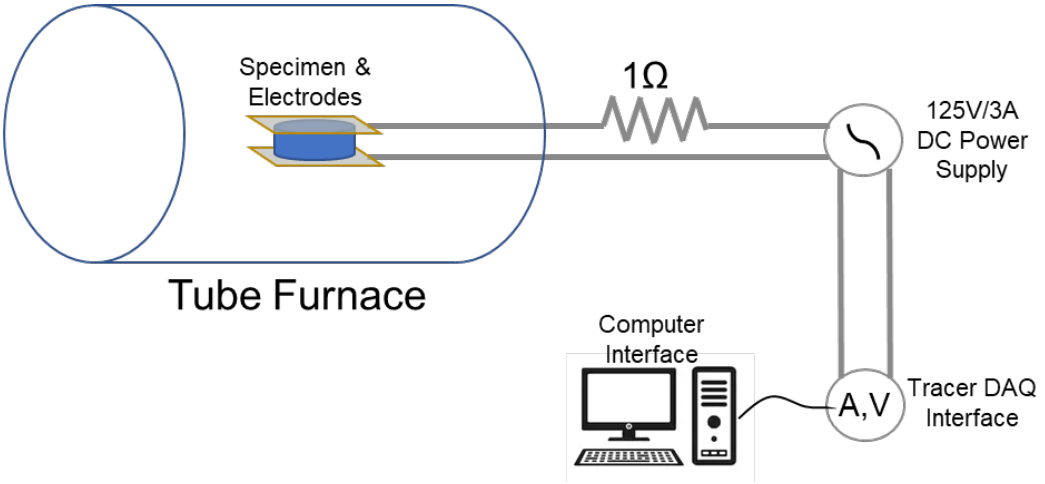

Fig. 5 Circuit diagram for the DC flash sintering apparatus

2.4 AC Flash Apparatus

A second flash system was used for experiments involving AC signals. This system, referred to as the AC flash system, consisted of an MTI OTF-1200X single-zone quartz tube furnace and a Keysight 6812c 750-W 300-V_{rms}/6.5-A AC/DC power supply. The tube ends were sealed using removable flanges, enabling experiments to be run under atmosphere, low vacuum, or inert gas. A 1-Ω resistor was placed in series with the circuit to provide base resistance. Open circuit resistance of the setup at room temperature was measured at 5.5 ± 2.5 Ω (95% confidence limit). Temperature profiles were controlled via set point programs entered into the built-in temperature controller. Temperature set point and thermocouple values

were recorded using MTI software and a custom LabVIEW interface with the furnace.

Applied voltage and maximum current were controlled with a custom-developed LabVIEW software interface. This interface was capable of applying a set voltage until maximum current was reached for temperature ramp experiments, or applying a voltage or current ramp until a set maximum current was reached for isothermal experiments. A DC voltage, AC voltage with configurable frequency and waveform, or combination of the two was applied. AC root mean squared (RMS) voltage and current, as well as DC offset voltage and current, were recorded from the power supply in situ using the LabVIEW software. The data was processed to remove the effects of the 1-Ω resistor during application of voltage to the specimen by subtracting the voltage drop across the resistor from the applied voltage to the system. A circuit diagram of the setup is provided in Fig. 6.

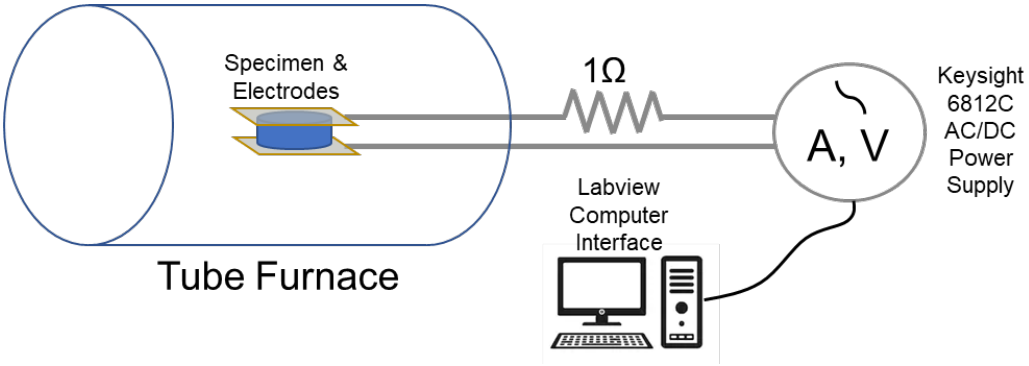

Fig. 6 Circuit diagram for AC flash sintering apparatus

2.5 Experimental Procedure

The following experimental procedure was used for all flash experiments, including both AC and DC setups. Each specimen was removed from the vacuum oven and weighed, with thickness and diameter measured using calipers. After selecting one of the electrode configurations described in Section 2.1, the specimen was inserted, and open circuit resistance was measured using a digital multimeter (DMM). Once the specimen and electrodes were set up, the tube furnace was closed, triple evacuated with a rough vacuum pump to at least –25 mmHg, and backfilled with ultra-high-purity argon unless an atmosphere of air was desired. The tube furnace was either evacuated for experiments under vacuum or backfilled with argon to atmospheric pressure with a slight overpressure bubbled through a bath of mineral oil to prevent backflow.

The desired temperature/voltage/current profile was applied to the specimen, as described in Section 2.2 for the DC flash setup and in Section 2.3 for the AC flash

setup. For experiments taking place at constant temperatures, the furnace was left at the hold temperature for 1 h to equilibrate the setup. DMM resistance measurements were taken immediately after voltage was removed from the specimen. Once the flash experiment was completed, the furnace was left to cool to room temperature, at which point a final DMM resistance measurement was taken. The specimen was then removed from the system for characterization.

2.6 Data Analysis

Raw data input consisted of the furnace temperature (as measured by the built-in thermocouple), power-supply output voltage, current, and time. To normalize voltage (V) and current (I) across specimens with different dimensions, the values were converted to electrical field (E) and current density (J) using the measured specimen thickness (t) and diameter (d), according to Eqs. 1 and 2.

$$E = \frac{V}{t} \tag{1}$$

$$J = \frac{I}{0.25\,\pi\,d^2} \tag{2}$$

Resistance (R) and resistivity (ρ) were calculated by dividing voltage by current, or electric field by current density, using Eqs. 3 and 4, respectively.

$$R = {}^{V}/_{I} \tag{3}$$

$$\rho = {}^{E}/_{J} \tag{4}$$

Power (P) and power density (p) were calculated by multiplying voltage and current, or electric field and current density, using Eqs. 5 and 6, respectively. Data was processed for each point in time. For some specimens, it was observed that the current was localized to a channel of unknown cross-sectional area through only a portion of the specimen. For these specimens, the current density, resistivity, and power density values were not reported, as the cross-sectional area was unknown.

$$P = I * V \tag{5}$$

$$p = E * J \tag{6}$$

2.7 Specimen Analysis

Postflash specimens were reweighed and thicknesses and diameters remeasured. Specimen density and porosity were calculated from the mass and dimensions using the theoretical density of B_4C. A combination of optical photography and scanning electron microscopy (SEM) was used to detect and image features of interest.

3. Results and Discussion

3.1 Initial Electrical Contact and Atmosphere Experiments

Initial trials for flash sintering of B_4C were performed using temperature ramps of 5 or 10 °C/min under a constant field strength of 280 V/cm, with varied electrode configurations and furnace atmospheres. Voltage was applied at room temperature, and the furnace temperature increased until the current reached 3 A, at which point the temperature and current were held for 5 min. The electrical power was then removed and the system cooled to room temperature.

The electrical contact type was varied among the four electrode configurations (TiB_2, graphite foil, graphite paste, and graphite foil in the graphite punch configuration), as described in Section 2.2, to determine if there was any effect from the electrode–specimen contact. Graphs of electric field, current, power, and temperature for each electrode type under an argon atmosphere are presented in Fig. 7. Collected data, including initial contact resistance, specimen resistance, and flash temperature, is presented in Table 1.

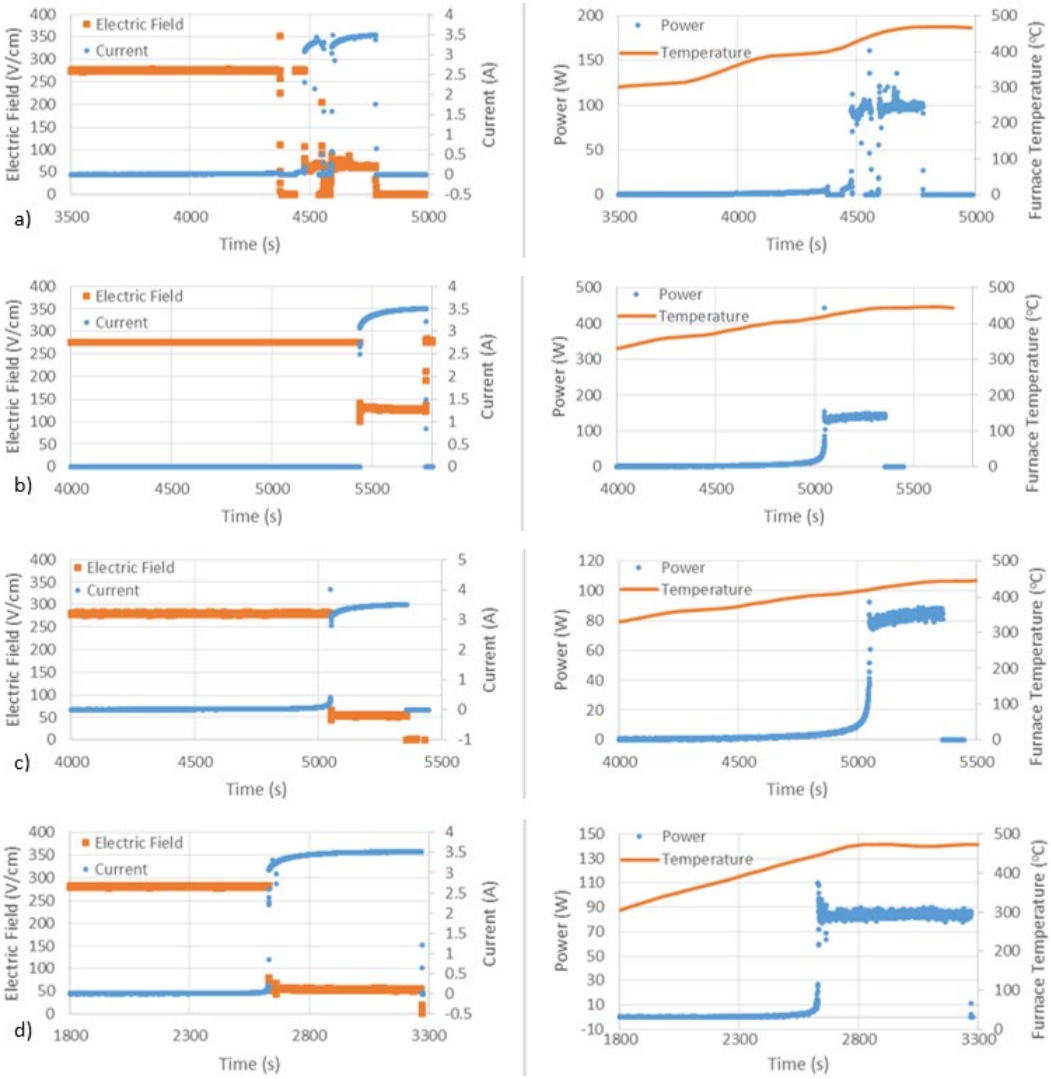

Fig. 7 Graphs of electric field, current, power, and temperature vs. time for a) specimen 1AR012-B4C-1 flash-sintered with TiB_2 electrodes, b) specimen 1AR012-B4C-2 flash-sintered with graphite foil electrodes, c) specimen 1AR017-B4C-1 flash-sintered with graphite foil electrodes after applying graphite paste to the specimen, and d) specimen 1AR191-B4C-1 flash-sintered with the graphite punch electrodes. All specimens were flashed in argon via temperature ramp under a constant DC field strength of 280 V/cm and a maximum current of 3 A.

Table 1 Summary of data from electrode and atmosphere experiments

Specimen	Electrode configuration	Atmosphere	Setup resistance (Ω)	Room temperature specimen resistance (MΩ)	Flash temperature (°C)	Final density (%)
1AR012-B4C-1	TiB_2	Argon	20.0	2.20	452	61.9
1AR012-B4C-2	Graphite foil	Argon	9.8	0.83	436	64.1
1AR017-B4C-1	Graphite paste	Argon	3.0	1.95	433	64.4
1AR191-B4C-1	Graphite punch	Argon	5.3	9.00	461	66.6
1AR028-B4C-2	Graphite foil	Air	5.0	1.80	517	68.1
1AR028-B4C-T4	Graphite foil	Vacuum	4.7	0.49	460	64.4

All specimens exhibited an exponential increase in current that initiated around 400 to 450 °C, culminating in a flash event during which the maximum current of the power supply was reached. A bright glow, characteristic of temperatures above 1500 °C, was observed through a window in the end cap of the tube furnace. Some variations in setup resistance and initial specimen resistance were noted, but the steady-state power (and thus resistance) during flash were consistent. Despite a classic flash event occurring, the overall density of the specimens had not significantly increased. Optical and SEM evaluation of the specimens revealed a thin channel of dense B_4C running from the positive to negative electrode in all three specimens. Cross-sectional SEM showed that the channels were approximately 50 μm deep and revealed gradients from fully dense regions, to partially dense regions exhibiting grain growth, to powders (Fig. 8).

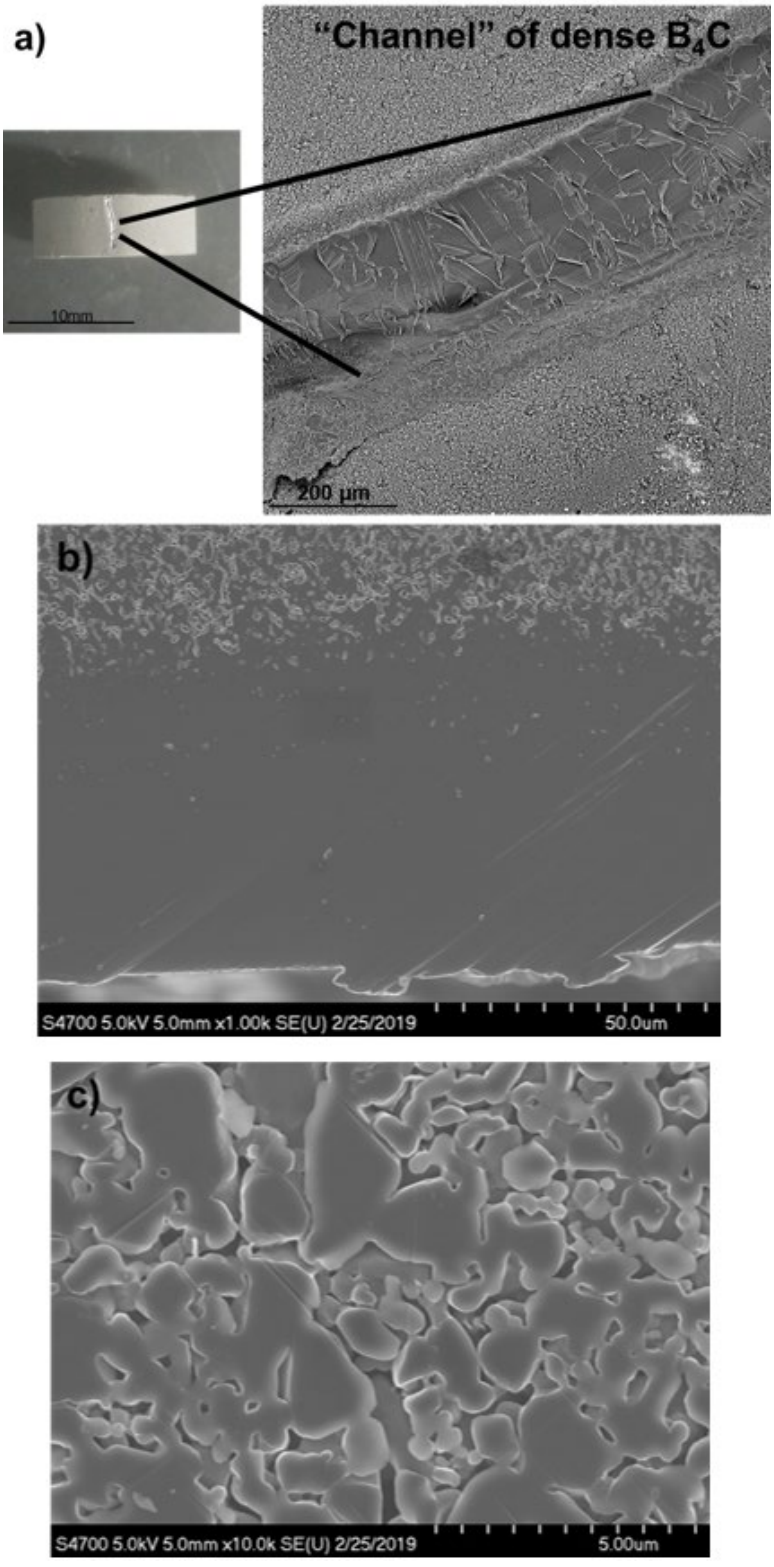

Fig. 8 Images of a flash-sintered specimen showing a) surface view of a channel via photograph and SEM, b) SEM cross section of the channel showing the gradient from fully dense (bottom) to porous (top), and c) SEM image of the partially dense region of the channel showing grain growth and densification

Additional experiments were conducted to evaluate if the chamber atmosphere had any significant impact on flash behavior. Temperature ramp DC flash experiments at field strengths of 280 V/cm were conducted in air and rough vacuum (approximately –30 mmHg) to test the extreme cases. Electrical and furnace temperature data for experiments under different atmospheres is plotted in Fig. 9 and additional data recorded in Table 1.

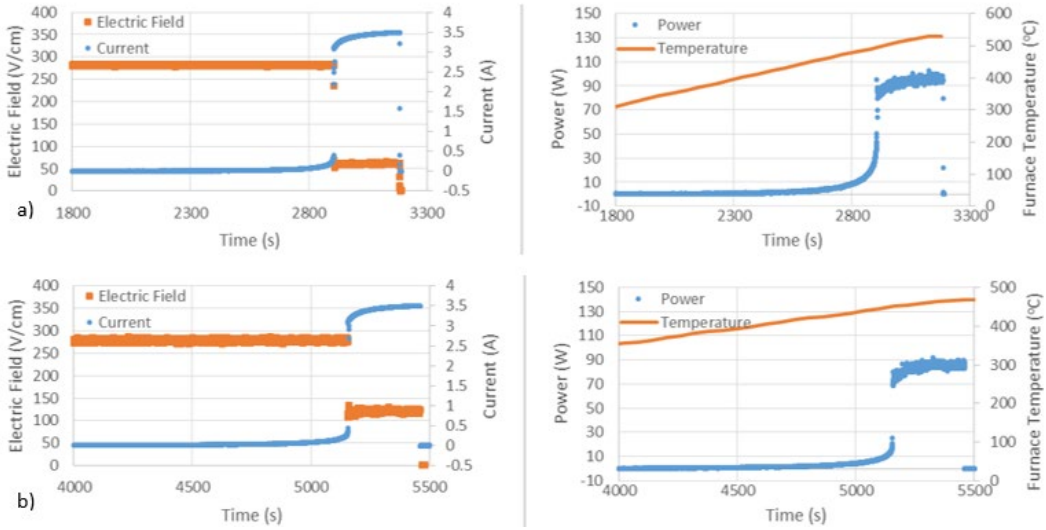

Fig. 9 Graphs of electric field, current, power, and temperature vs. time for a) specimen 1AR028-B4C-2 flash-sintered in air, and b) specimen 1AR028-B4C-T4 flash-sintered in vacuum. All specimens were flashed with graphite foil electrodes via temperature ramp under a constant DC field strength of 280 V/cm and maximum current of 3 A.

Significant differences in flash temperature or behavior were not observed for the experiments conducted under different atmospheres. Evaluation of the specimens revealed that all of them formed channels. The channels in the specimens flashed in air ran through the specimen center as opposed to those flashed under inert environments in which the channels traced the outer edges. The specimens flashed in air exhibited increased surface oxidation, which was expected given that B_4C starts to oxidize at temperatures as low as 550 °C.[20]

These initial experiments led to several conclusions. First, the observations of grain growth and fully densified regions indicated that flash sintering of B_4C to full density at temperatures as low as 433 °C was possible. While changes in powder morphology, size, and composition are known to influence flash behavior, these results demonstrated that densification was possible with the powder and compaction methods used in these sets of experiments. However, the localized nature of the densification also showed that current flowed preferentially through only a small portion of the specimen rather than uniformly throughout. The channel

of hot, dense B_4C acted as an electrical short, preventing homogenous densification of the entire specimen. Practical application of flash sintering B_4C requires scaling the densification within the channel to the entire volume of a specimen as opposed to an isolated portion.

The lack of response to variation of contact type or atmosphere indicated that current channeling was not caused by electrical contact, chemical compatibility of the electrodes, or the atmospheric environment. Published research on similar "hot spot" and channeling behavior in oxide ceramics has demonstrated several ways to avoid current localization.[6] Alterations to the electric field strength, current density, and flash temperature as well as application of a voltage or current ramp to avoid a large power spike during flash were theorized to be methods to prevent formation of a channel and evenly distribute temperature and densification throughout the specimen.

3.2 DC Design of Experiment (DOE)

A DOE was generated to probe two potential routes for preventing channel formation during flash sintering of B_4C. Based on the conclusions from Section 3.1, the variables selected for investigation were ramp type, electrical "power" (defined as the product of electrical field and current density), and flash temperature. DOE experimental parameters and high/low settings are given in Table 2. A 2^{3-1} fractional factorial design with three factors varied across four runs was used. Ramp type was varied between a 5 °C/min temperature ramp at constant applied electric field and a 2.22 V/(cm*s) voltage ramp at constant temperature. All specimens were sintered in the DC flash setup using graphite foil electrodes in the alumina-brick configuration and an argon-flow atmosphere. Power and temperature were maintained for 5 min after maximum current was reached and removed to allow furnace cooling to room temperature.

Table 2 Experimental settings for the DOE

Specimen	Ramp type	Temperature profile	Applied voltage	Specimen dimensions	Electric field	Current density
1AR017-B4C-1	Temperature	5 °C/min to flash	125 V	4.5 mm × 12.8 mmØ	278 V/cm	3.0 A
1AR017-B4C-4	Temperature	5 °C/min to flash	31 V	4.5 mm × 12.8 mmØ	70 V/cm	3.0 A
1AR017-B4C-2	Voltage	450 °C	1 V/s to flash	4.5 mm × 12.8 mmØ	0.22 V/(cm*s)	2.3 A/cm^2
1AR017-B4C-3	Voltage	550 °C	1 V/s to flash	4.5 mm × 28 mmØ	0.22 V/(cm*s)	0.5 A/cm^2

The physical differences between the voltage ramp and temperature ramp experiments drove the selection of the other variables. For the temperature ramp experiments, “power” was varied by altering the field strength, as current density could not be controlled. A high setting of 278 V/cm was selected for consistency with the experiments in Section 3.1. A low setting of 69 V/cm was selected because it was only slightly above the typical field strength during flash. Flash temperature was not directly controllable in temperature ramp experiments but anticipated to be higher for low field strength (power).

For experiments with voltage ramps at constant temperatures, power was controlled by changing the current density via cross-sectional area because the DC power supply was not capable of directly controlling current. The diameter of the specimens was varied between 13 and 25 mm, increasing the cross-sectional area by roughly four times. A low furnace temperature setting of 450 °C was selected to replicate the flash temperature during temperature ramp experiments, and a high setting of 550 °C was selected to match the anticipated furnace temperature during the low-power temperature ramp experiments.

While these experimental settings were confounded with each other, the range of settings covered a wide span of thermal and electrical parameters targeted to identify regions in which flash could occur without forming a channel. Results are summarized in Table 3. Both temperature ramp specimens flashed in a similar manner and formed distinct channels along their outer edges as observed by visual and SEM inspection. Electrical and temperature data for these two specimens is plotted in Fig. 10. As the 70-V/cm electric field was only slightly higher than the field strength during flash (approximately 50–60 V/cm), it was concluded that barring other experimental changes, specimens flashed with a temperature ramp constant voltage profile always formed channels.

Table 3 Summary of critical DOE data collected

Specimen	Specimen resistance	Dimensions	Flash Temp	Flash voltage	Postflash resistance	Density change	Channel formed?
1AR017-B4C-1	1.95 MΩ	4.5 mm × 12.8 mmØ	433 °C	125 V	28.8 Ω	–0.6%	Yes
1AR017-B4C-4	2.70 MΩ	4.5 mm × 12.8 mmØ	550 °C	31 V	20.4 Ω	0.5%	Yes
1AR017-B4C-2	1.42 MΩ	4.5 mm × 12.8 mmØ	450 °C	70 V	13.6 Ω	0.9%	Yes
1AR017-B4C-3	2.07 MΩ	4.5 mm × 28 mmØ	550 °C	40 V	28.0 Ω	–0.2%	No

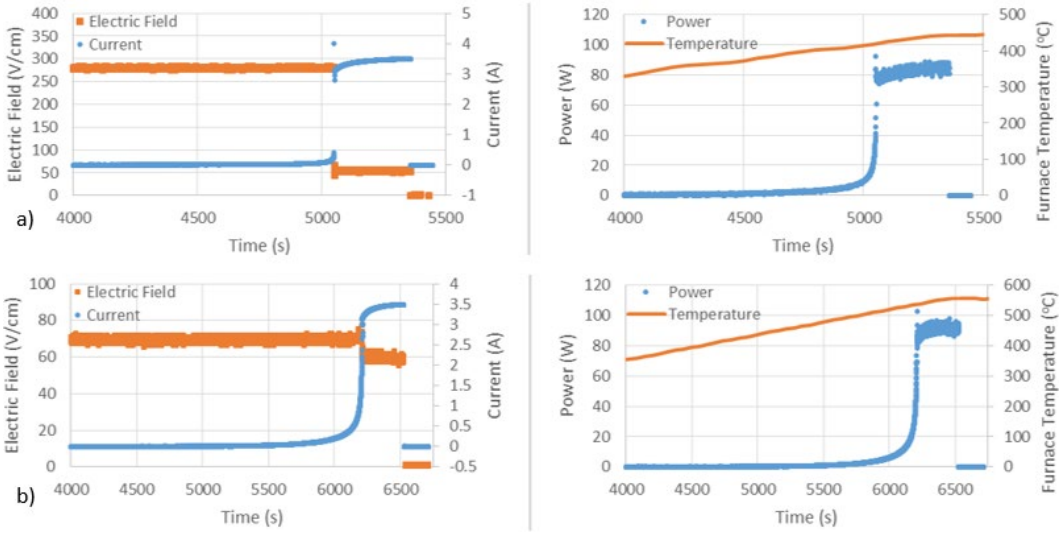

Fig. 10 Electric field, current power, and temperature measurements for specimens a) 1AR017-B4C-1 with a 278-V/cm field strength, and b) 1AR017-B4C-4 with a 69-V/cm field strength. Both specimens were heated at 5 °C/min until flash, with power and temperature held for 5 min once maximum current was reached.

Of the two specimens flashed with a voltage ramp at constant temperature (Fig. 11), the 13-mm-diameter specimen flashed at 450 °C and exhibited channel formation, though the channel passed through the interior of the specimen as opposed to along the surface. The 28-mm-diameter specimen flashed at 550 °C, did not form a channel, and was observed to flash with a dull red glow as opposed to a bright, concentrated light, indicating a substantially lower specimen temperature. However, there was no appreciable volumetric densification of the specimen indicated by specimen dimensions and density measurements.

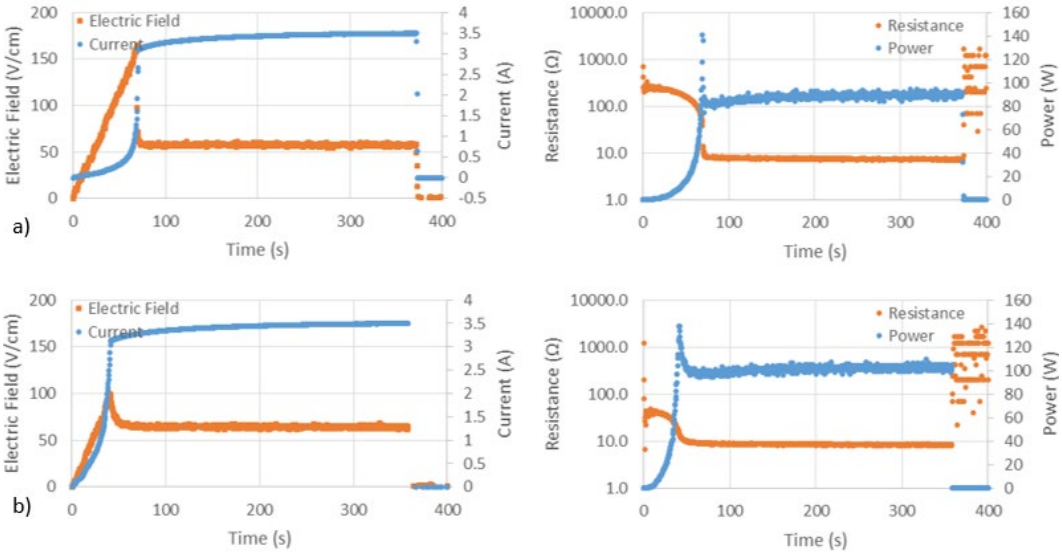

Fig. 11 Electric field, current, resistance, and power measurements for specimens a) 1AR017-B4C-2 flashed at 450 °C with a 1-V/s voltage ramp, and b) 1AR017-B4C-3 flashed at 550 °C with a 1-V/s voltage ramp. Both specimens were held at temperature for 1 h prior to application of voltage.

Electrical power during flash was similar for all specimens at 80, 86, 86, and 100 W, respectively. The resistance during flash ranged from 7 to 10 Ω. This was significantly higher than the circuit load of 1 Ω, and assuming additional line resistance was not greater than 1 Ω, approximately 80% to 90% of the power was absorbed by the specimen. This supported observations that electrical contact was not a significant factor, as poor or variable contact would be reflected as variable resistance during flash. Specimen 1AR017-B4C-3 had a similar resistance to the other specimens, despite being much larger and flashing more uniformly, as opposed to channeling. This could be explained by the geometric interplay between resistance and resistivity in Eq. 7:

$$R = \rho(l/A) \tag{7}$$

where R is resistance, ρ resistivity, l specimen thickness, and A specimen cross-sectional area. The identical resistance and thickness of the specimens indicated that the ratio of resistivity to area must be constant, which fit the observations of high specimen temperature (low resistivity) and channeling (low area) in specimens that channeled, and low specimen temperature (high resistivity) and lack of channeling (high area) in the specimen that did not.

Observation that higher temperatures and lower current densities prevent channeling was consistent with the behavior observed by Trombin and Raj,[16] and subsequent experiments with 13-mm-diameter specimens confirmed that the increased temperature, not the specimen size, was critical for preventing

channeling. However, densification, local or otherwise, was not observed in the specimens where channeling did not occur. Infrared camera measurements were made using a FLIR T540 during flash. Results indicated that the specimen reached a temperature of only approximately 800 °C, indicating the temperature of the specimen was not nearly comparable to conventional sintering temperatures for B_4C (typically 1800–2200 °C). Based on these observations, and compared with the small interaction volume in the channeling case that successfully densified the powder, it was concluded that the power density in the nonchanneling case was not high enough to heat the sample to temperatures where sintering could occur. This is likely an inherent challenge to B_4C, as the power dissipated during flash sintering is proportional to the material resistivity, which is significantly lower for B_4C compared with oxide ceramics.

3.3 Coefficient of Variation (COV) Study

Prior to proceeding, a COV study was designed and executed to establish the baseline variability of factors measured in the experiments and to identify potential uncontrolled experimental factors affecting flash behavior. A process flowchart for the flash sintering setup is shown in Fig. 12 with potential factors separated into "controlled" and "uncontrolled". A COV tree was designed in Fig. 13 with pellet batch, electrical contact, ramp type, and specimen number selected as factors. The design was intended to answer several critical questions, including:

- Are there significant variations in the properties of B_4C pellets used for flash experiments?
- Are flash experiments affected by time-related environmental factors, such as humidity?
- Is there a detectable difference between flash behavior using graphite foil and TiB_2 electrodes?
- How consistent is the flash temperature?
- How consistent is the presence or absence of channeling?
- What is the variability in output measurements for experiments conducted under the same conditions?

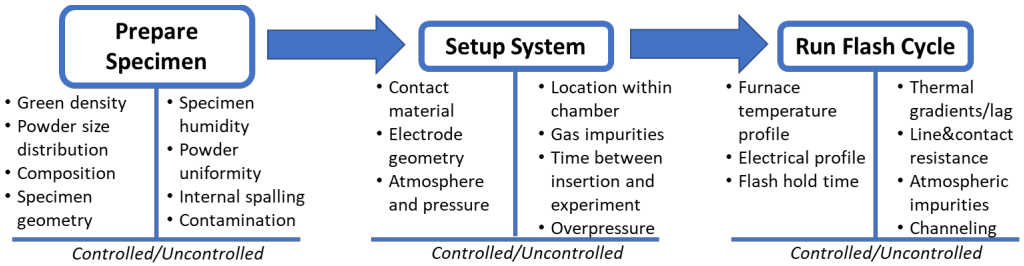

Fig. 12 Process flowchart for flash sintering showing "controlled" and "uncontrolled" factors

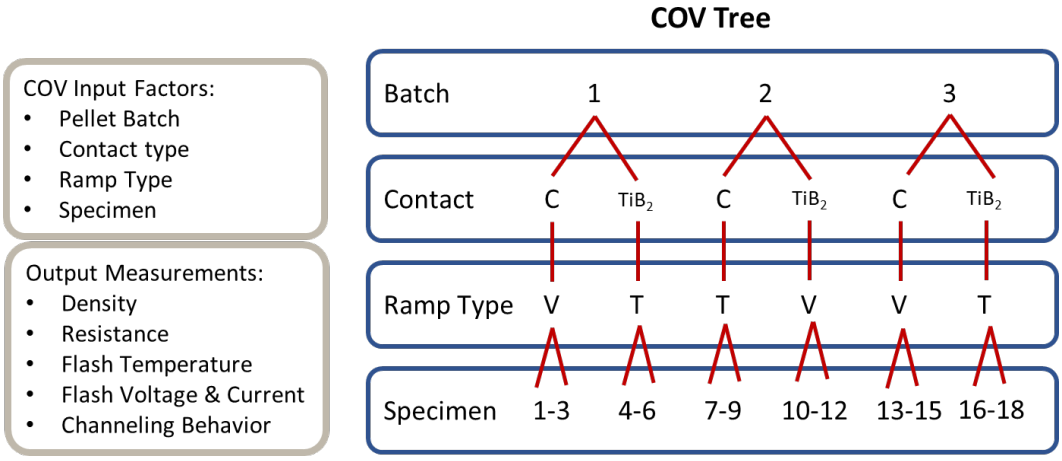

Fig. 13 COV design and factor tree

Experiments were conducted across an 8-month time period using the DC flash-sintering setup. Standard 1-g, 13-mm-diameter by 4.5-mm-tall cylindrical specimens were prepared as described in Section 2.1. The two electrode configurations used were graphite foil with alumina bricks and TiB_2 cylindrical electrodes. All experiments were performed in an argon atmosphere with either a voltage ramp at constant temperature or temperature ramp at constant voltage. Voltage ramp experiments used ramp rates of 0.1 V/s at 550 °C with a 1-h soak time at high temperature prior to application of voltage to bring the furnace to thermal equilibrium. Temperature ramp experiments used heating rates of 5 °C/min under an applied field strength of 278 V/cm. Current and temperature were maintained for 5 min once the flash conditions of maximum current (3 A) were reached. Experimental data was measured and recorded as described in Section 2.3.

3.3.1 Pellet Green Density

The pellet green density measurements had an overall average density of 65.6% with a standard deviation of 0.8%. Densities followed a Gaussian distribution, with a p-value of 0.595 (Fig. 14a). Variation from batch to batch was analyzed by plotting the mean and expected ranges (an Xbar-R control chart). The batch mean

and range remained within the 95% probability bounds as determined by the range of pellet densities (Fig. 14b). This indicated that the pellet pressing process produced specimens with average densities of 65.6% with 95% confidence limits of 1.6% from the mean.

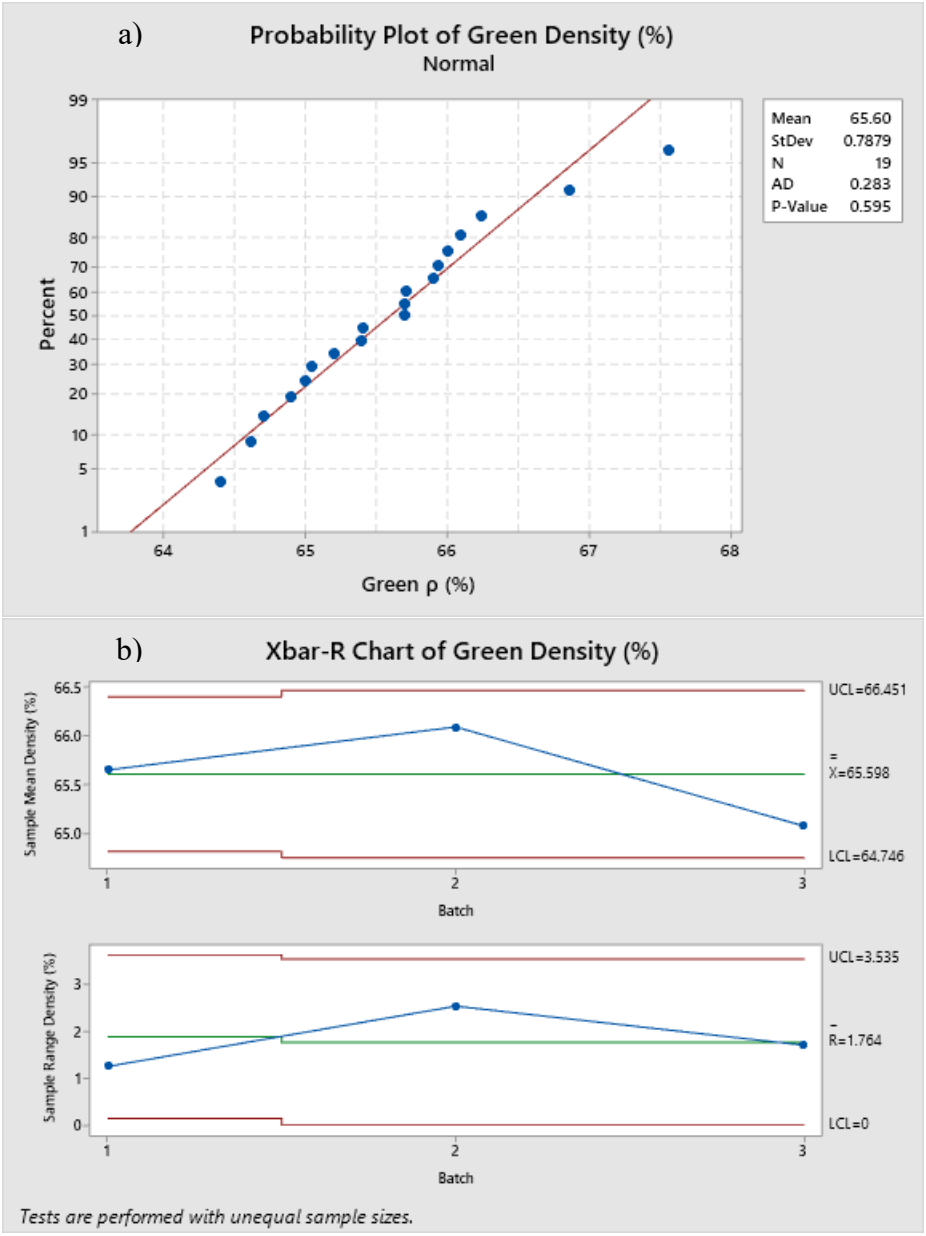

Fig. 14 a) Probability plot of green densities and b) mean and range density charts for pellet green densities sorted by batch

3.3.2 Resistance Measurements

Setup and contact resistances did not follow a normal or lognormal distribution, with three outliers at high resistance disturbing an otherwise normal distribution (Fig. 15). All three were with the TiB_2 electrode setup, indicating that the electrical contact of the TiB_2 electrodes was not as good as the graphite foil electrodes. This was attributed to the hard surface of the TiB_2 electrodes, which could not conform like the graphite foil and were harder to connect to the chromel wires. Initial specimen resistance was consistent across the COV branches as a function of the electrode type (Fig. 16). Resistance with graphite foil electrodes was typically around 1 MΩ, while the specimens using TiB_2 electrodes were typically at or above the maximum range of the DMM (40 MΩ). The specimen in Branch 3 was processed using TiB_2 electrodes with a circular punch-out of graphite foil placed between the TiB_2 electrode and the specimen to act as the electrical contact. This configuration allowed the effects of electrical contact to be isolated from those of the electrode's thermal and physical properties.

The electrical resistivity of powder compacts has been shown to decrease with mechanical load,[21] and the mass of the graphite foil electrodes was significantly higher than that of the TiB_2 electrodes. For the specimen with the hybrid TiB_2–graphite foil electrodes, the resistance was still higher than the specimens in the graphite foil electrodes but lower than the other TiB_2 specimens, indicating that both pressure and the electrode–specimen interface significantly affected specimen resistance. Overall, based on the measured open-circuit resistances and the resistances with the specimen inserted, both electrode configurations produced reasonably reproducible initial resistances, with lower specimen resistances in the graphite foil electrodes due to effects of both interfacial resistance and mechanical load.

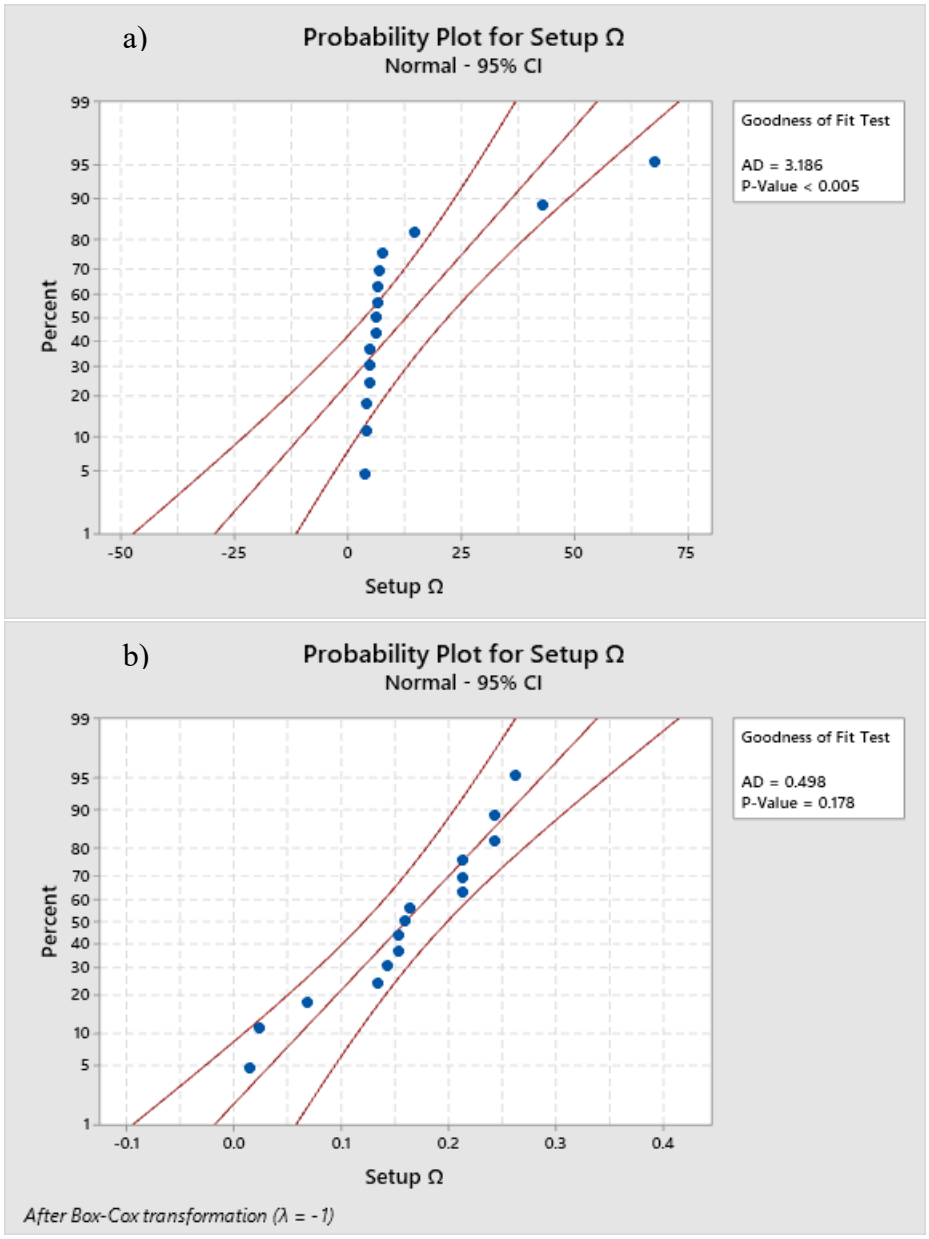

Fig. 15 Setup resistance probability plot for a) all specimens and b) all specimens with outliers removed

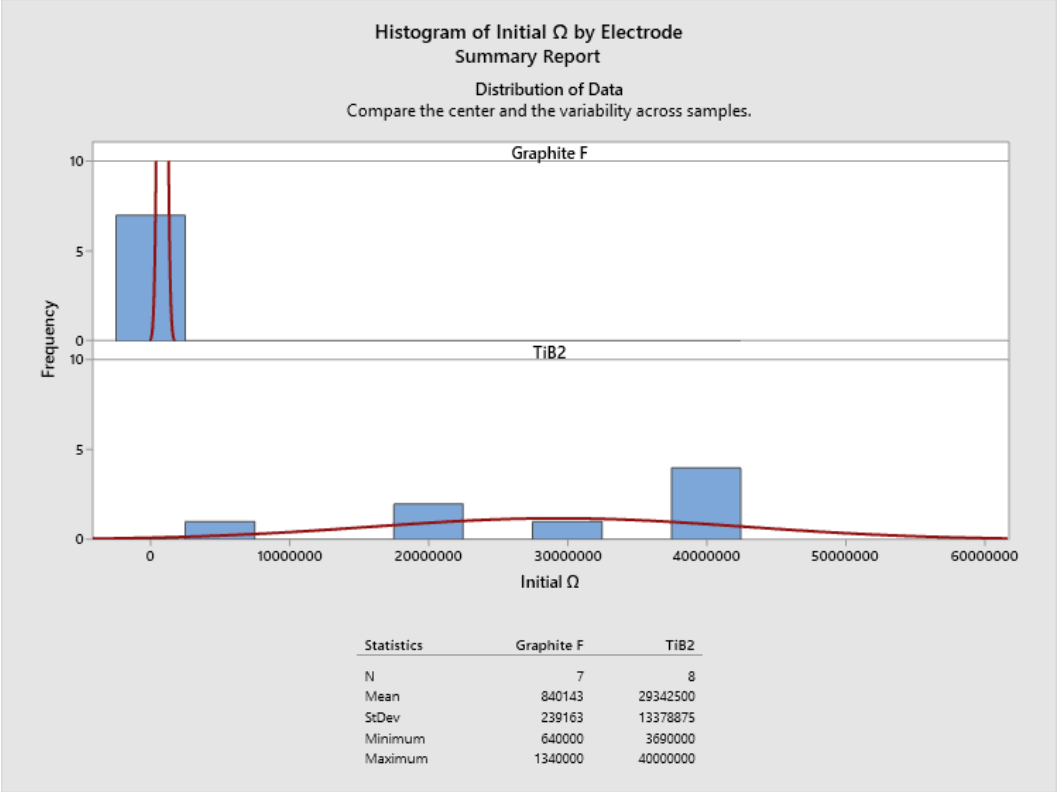

Fig. 16 Histogram of initial specimen resistance by electrode type

Resistance after flash at elevated temperatures and room temperatures was higher in specimens with TiB_2 electrodes than those with graphite foil electrodes (Fig. 17). Similar to the pre-flash resistances, these differences were attributed to the effects of thermal expansion combined with the ability of graphite foil to deform and maintain contact with the specimen. Repeated measurements of resistance after flash at high temperatures observed that the resistance rapidly increased immediately after power was removed from the system, likely due to rapid temperature drop, rendering the measurements of questionable accuracy.

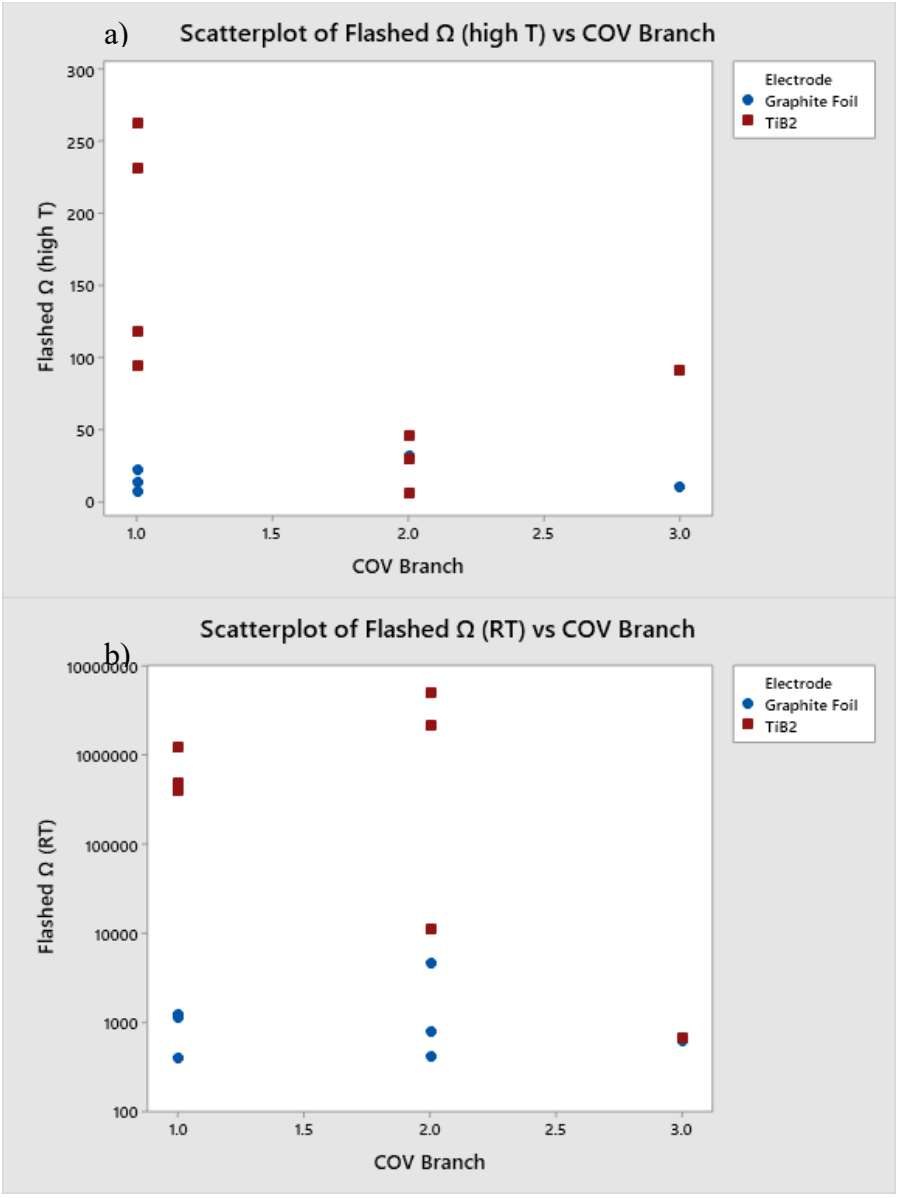

Fig. 17 Specimen resistance after flash at a) high temperatures less than 2 min after power was removed and b) room temperature

3.3.3 Temperature Ramp Results

Flash temperature is plotted against specimen batch and electrode type in Fig. 18. The mean flash temperature of specimens in the graphite foil configuration was 422 °C with a range of 44 °C compared with 385 °C with a range of 22 °C for specimens sintered with TiB_2 electrodes. A two-sample T-test across electrode types gave a p-value of 0.115, which indicated an 88.5% probability of a difference but was above the 0.05 level required for statistical certainty. The 95% confidence limit boundaries of the difference between TiB_2 and graphite foil electrodes were 22.2 and 96.6 °C.

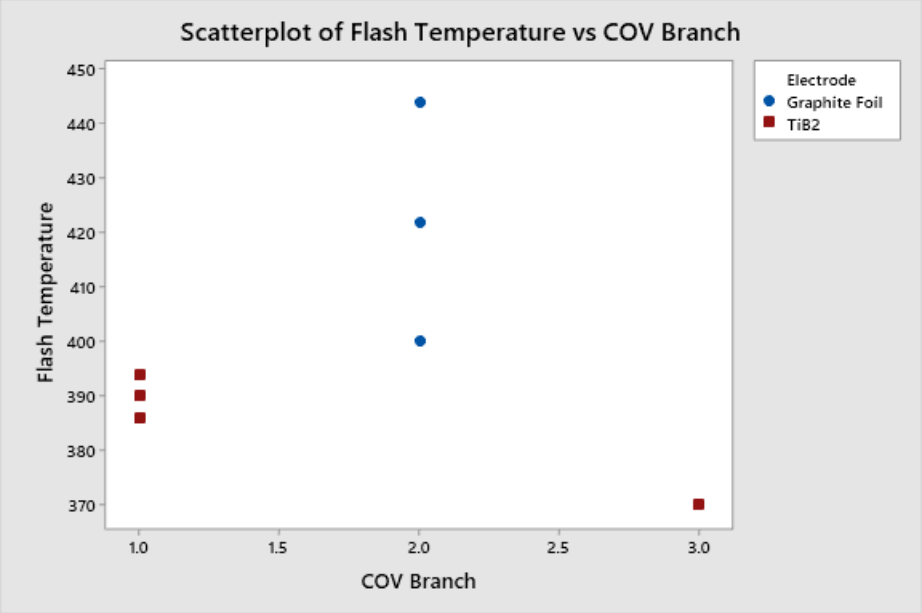

Fig. 18 Flash temperatures for specimens flashed at constant field strength (278 V/cm) and a 5 °C/min temperature ramp

Graphs of electric field, current, power, resistance, and temperature versus time are plotted in Fig. 19, and Table 4 summarizes temperature ramp flash data. All of the specimens exhibited channeling, with the channel pathway passing along the edge of the specimen in each case. Current density, power density, and resistivity were not calculated for these specimens, as the cross-sectional area of the channel was not well known. Flash behavior was highly reproducible, with similar power densities and electric field strengths during flash regardless of specimen, flash temperature, or electrode type.

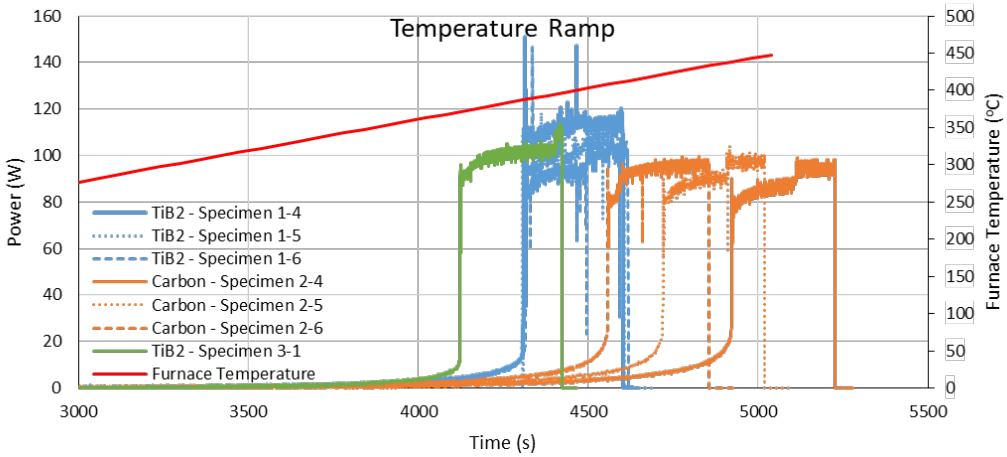

Fig. 19 Power and temperature measurements for all specimens flashed with a temperature ramp

Table 4 Summary of temperature ramp flash data

Specimen	Flash date	Green density (%)	Electrode	Setup resistance	Specimen resistance (MΩ)	Mass change (g)	Density change (%)	Flash temp. (°C)	Avg. flash power (W)	Avg. flash resistance (Ω)	Channeling?
1AR059-B4C-4	6/21/2019	66.0	TiB_2	6.3	40.0	–0.011	–0.7	386	110	9.5	Yes
1AR059-B4C-5	6/25/2019	65.2	TiB_2	7.0	40.0	–0.003	0.1	394	102	8.6	Yes
1AR059-B4C-7	7/2/2019	65.0	TiB_2	7.5	20.0	–0.001	0.0	390	95	8.0	Yes
1AR097-B4C-COV-2	8/5/2019	67.6	Graphite foil	6.1	0.86	–0.002	–1.2	444	89	7.5	Yes
1AR097-B4C-COV-4	10/15/2019	65.4	Graphite foil	4.7	0.64	0.004	0.2	422	94	7.6	Yes
1AR097-B4C-COV-6	11/13/2019	65.0	Graphite foil	4.1	0.66	–0.005	–0.3	400	93	7.7	Yes
1AR140- COV-2	11/21/2019	65.7	TiB_2	42.9	3.69	–0.002	–0.4	370	100	8.5	Yes

The TiB_2 and graphite foil electrodes behaved similarly, though the flash temperature was likely slightly lower when using TiB_2 electrodes. This would make physical sense, as the TiB_2 electrodes had lower thermal mass and a higher thermal conductivity than the graphite foil electrodes (which were wrapped around an alumina brick). Therefore, the local temperature of the graphite foil electrodes should have lagged somewhat behind the measured furnace temperature when operating with a temperature ramp, resulting in a higher measured flash temperature. The higher variability in flash temperature of the graphite foil electrode configuration could have been attributed to an increased sensitivity to specimen location within the tube furnace (an uncontrolled variable).

The overall flash temperature appeared to vary by at least ±22 °C under normal experimental conditions, indicating that when operating across multiple experiments and electrode configurations, a range of flash temperatures from 350 to 475 °C should be expected. However, the actual physical temperature of the specimen at which flash occurred was likely substantially more consistent than the furnace temperatures. Based on the similarities in electrical data and channeling behavior, there appeared to be no significant differences between the flash behaviors in any of these runs. Therefore, while improved local temperature measurements could be beneficial, temperature-ramp-style flash experiments should be expected to have reproducible outcomes when performed with different pellets, times, or electrode types.

3.3.4 Voltage Ramp Results

The results from all specimens flash-sintered using a voltage ramp profile are summarized in Table 5. A slight mass gain up to 0.03 g was observed, attributed to oxidation during the 1-h soak at 550 °C. Electrical measurements plotted against time are presented in Fig. 20. All specimens flashed with near-identical power curves at electric fields within a range of 86 to 105 W. There was no significant difference between the power curves of specimens flash-sintered with graphite foil and TiB_2 electrodes, though a slight increase in the incubation time between the application of voltage and flash may have been present. However, the electrode type strongly impacted channeling behavior. All specimens flashed with TiB_2 electrodes formed a channel through the center of the specimen (as opposed to the edge during temperature ramp experiments), while the specimens flashed with graphite foil electrodes did not.

Table 5 Summary of COV data from voltage ramp experiments

Specimen	Flash date	Green density (%)	Electrode	Setup resistance (Ω)	Specimen resistance (Ω)	Mass change (g)	Density change (%)	Avg. flash power (W)	Avg. flash resistance (Ω)	Channeling
1AR059-B4C-1	5/16/2019	66.2	Graphite foil	4.7	0.71	0.0016	–0.3	86	7.3	No
1AR059-B4C-2	5/20/2019	65.9	Graphite foil	4.7	0.88	0.0123	0.6	95	8.2	No
1AR059-B4C-3	6/5/2019	65.7	Graphite foil	3.8	0.79	0.0	0.9	92	7.9	No
1AR097-B4C-COV-1	8/2/2019	66.9	TiB_2	14.6	22.1	0.0268	2.8	102	9.0	Yes
1AR097-B4C-COV-3	10/10/2019	65.7	TiB_2	68.0	>40	0.0167	1.7	95	8.5	Yes
1AR097-B4C-COV-5	11/12/2019	65.9	TiB_2	6.5	>40	0.0298	1.2	105	9.0	Yes
1AR140-COV-1	11/20/2019	64.6	Graphite foil	4.1	1.34	0.0155	1.5	94	8.1	No

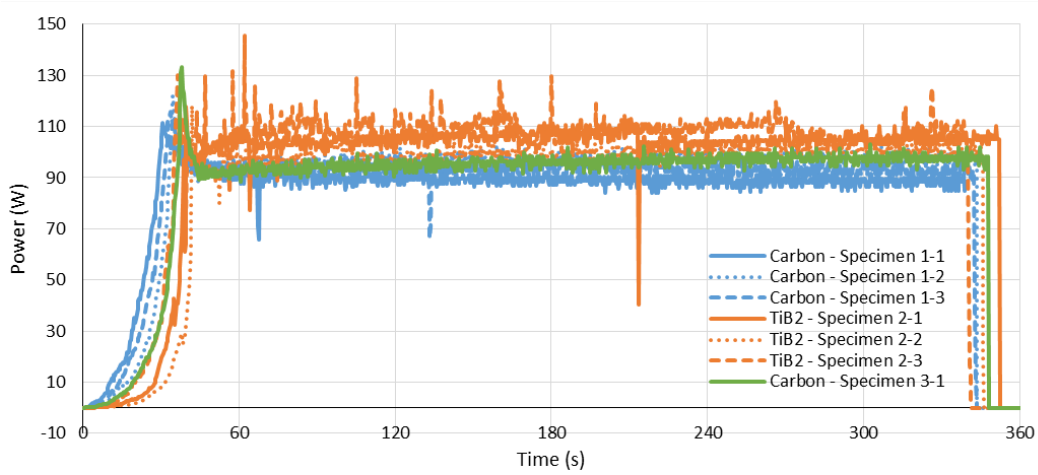

Fig. 20 Power measurements for all specimens flashed via a voltage ramp

Previously noted differences between the TiB_2 and graphite foil electrodes may explain the variation in channeling behavior. The TiB_2 electrodes had a hard, nonconforming surface with slightly higher contact resistance and a lower weight than the graphite foil electrodes, which may have made it easier for current to localize due to the intimacy of electrical contact and the effect of load on resistivity. Different thermal conductivities and masses of the system may have also played a role. However, comparison of the thermal conductivities for the two setups was difficult. The graphite foil was highly thermally conductive but thin and wrapped around a low thermally conductive alumina brick, making the overall thermal conductivity low but still promoting thermal dissipation from the specimen. The TiB_2 electrodes were uniformly highly thermally conductive, which increased thermal dissipation from the specimen relative to the graphite electrodes but had less thermal mass.

3.3.5 COV Conclusions

The COV study showed a high level of reproducibility in the flash experiments. Green specimen densities, the resistance of the setup, and electrical behavior of the flash phenomenon were consistent across the three specimen batches. Channeling, the most critical phenomenon observed in these studies, was also consistent within each ramp and electrode type. Anomalous effects from uncontrolled variables such as environmental factors, time, or the individual setup, were not more significant than run-to-run variability or other controlled factors. Therefore, it was concluded that future flash experiments should exhibit a high reproducibility, as long as they are conducted in an identical manner. This is particularly relevant for DOE-style experiments, as the COV results indicated that duplicate runs with identical conditions were not necessary to determine the effects on channeling behavior.

3.4 AC DOE

3.4.1 Experimental Design

The newly acquired AC power supply was used in a follow-on DOE designed to probe the influence of AC waveforms on flash behavior and to increase densification. From the previous results, it was hypothesized that the B_4C specimens had the potential to be flash-sintered to full density, as exhibited by the densification of the channels in Section 3.1, but that the lower power density in the nonchanneling voltage ramp experiments was preventing densification of larger volumes of the material. As such, the variables selected for DOE levels were AC versus DC waveform, furnace temperature, voltage versus current ramp, and specimen size. A $2^{(4-1)}$-type DOE matrix with four factors varied across eight runs was developed (Table 5). Settings were selected to either replicate the conditions in previous experiments or to provide a high power density to the specimen, with the maximum current set to 6 A as opposed to the 3-A limit of the DC power supply (Table 6). Temperature ramps were not explored further because they were considered a dead-end for obtaining uniform densification. Graphite foil was used for electrical contact, with the graphite punch in an alumina sleeve configuration used for easier handling of specimens during furnace insertion. Electrical measurement data, final densities, and the presence or absence of channeling were recorded as outputs.

Table 6 DOE parameters and other experimental settings

Variable	Low	High
AC/DC	DC	AC, 60 Hz
Ramp type	Voltage	Current
Ramp rate	33 mV/s, 3 mA/s	
Maximum current	6 A (RMS)	
Soak time	15 min	
Temperature	550 °C	1100 °C
Area	6 mmØ	13 mmØ
Thickness	4.5 mm	
Atmosphere	Argon	
Material	B_4C	
Powder size	~2 µm	
Electrode	Graphite foil	

3.4.2 Results and Discussion

Results are tabulated in Table 7, with power plotted against time in Fig. 21. Overall, none of the specimens exhibited densification, though some had a slight weight gain attributed to oxidation events at higher temperatures. Electrically, the

maximum power dissipated was higher at 550 °C and reduced by approximately half at 1100 °C, likely due to higher electrical conductivity at 1100 °C. There was no significant difference between AC and DC waveforms, as temperature and voltage ramps behaved similarly at 1100 °C, but at 550 °C, voltage ramps exhibited the classic power-spike characteristic of flash events.

Table 7 Summary of the AC DOE results

Run	AC/DC	Ramp type	Furnace temperature	Specimen diameter	Density change	Channeling?
1	AC	Current	550 °C	6 mm	2.4%	No
2	DC	Current	1100 °C	6 mm	4.0%	No
3	DC	Voltage	550 °C	6 mm	5.3%	Yes
4	AC	Voltage	1100 °C	6 mm	5.0%	No
5	DC	Current	550 °C	13 mm	2.8%	Yes
6	AC	Current	1100 °C	13 mm	3.8%	No
7	AC	Voltage	550 °C	13 mm	2.5%	Yes
8	DC	Voltage	1100 °C	13 mm	3.2%	No

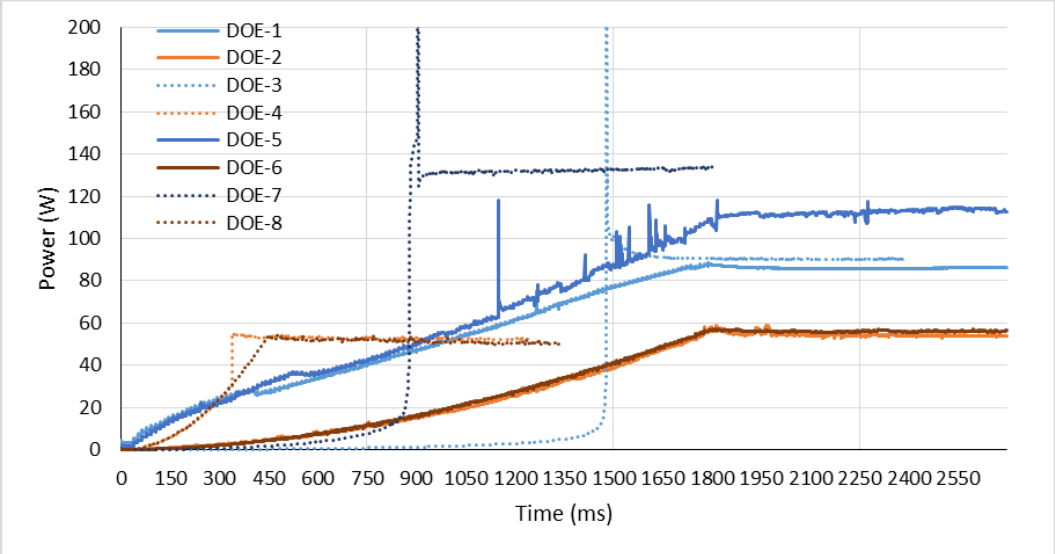

Fig. 21 Power (watts) vs. time for all specimens in the AC DOE listed in Table 7. Experiments at 1100 °C shown in red, and experiments at 550 °C shown in blue.

Temperature had the greatest influence on channeling (Fig. 22). None of the specimens flashed at 1100 °C formed channels, while three out of four at 550 °C did. This was consistent with literature reports that the "safe" zone for flash sintering covered a wider range of electrical settings at higher temperatures.[16] Out of the specimens sintered at 550 °C, only the 6-mm-diameter specimens sintered with an AC current ramp did not form channels, indicating that this combination of parameters was most favorable for avoiding channel formation.

Fig. 22 AC DOE specimens from Table 7 after flash showing formation or absence of channels

Despite exploring a wider range of furnace temperatures, higher current limits with the AC power supply, and smaller specimen sizes, none of the specimens exhibited significant uniform densification after flash sintering. Based on the similarities between AC and DC waveforms, there was no significant benefit from using an AC current for flash sintering of B_4C within the explored parameter space. Since B_4C does not have oxygen vacancies, the benefits of reduced gradient formation with AC observed in oxide ceramics[11–13] will not be present. Additional information was obtained on how to control channeling with furnace temperature, the power application curve, and specimen size identified as influential factors in this study.

4. Conclusions

Flash sintering was investigated as a method for densifying B_4C. Initial experiments across electrode type and atmosphere found that B_4C exhibited behavior similar to literature reports on flash sintering of oxide materials. However, due to extreme hot-spot formation localizing current and high temperatures, only a small portion of the specimen in the form of a thin channel, typically along the edge of the sample, was densified. A DOE was executed to investigate the influence of flash parameters and specimen size on channeling and densification. Changing from a temperature ramp at constant voltage profile to a voltage ramp at constant temperature profile prevented channel formation but resulted in a substantially lower temperature rise during the flash event, which did not result in any densification within the specimens.

A COV study was performed to evaluate the reproducibility of experiments and variation in key measured parameters. A high reproducibility in flash outcomes was

observed, and the variability in setup and specimen resistance, flash temperature, power measurements, and specimen densities were quantified. Pellet variations, setup and specimen resistance, and environmental effects were ruled out as significant sources of experimental variation, while electrode type was found to have significant effects on resistance, flash temperature, and channel formation.

A follow-on DOE study investigated the effects of AC current, specimen size, current ramp, and high temperature on channel formation and densification. Experiments confirmed the effect of temperature on channel formation, and uncovered slight effects from specimen size, ramp type, and current type. Volumetric densification of the entire specimen was not achieved across any of the experimental conditions evaluated. The difficulty in uniformly densifying B_4C was attributed to a combination of insufficient power density from the power supply, high thermal loss from the electrode configuration, and the inherently high electrical conductivity of B_4C. Potential future routes for obtaining volumetric densification of B_4C without channel formation via flash sintering include using a power supply capable of producing higher currents, further increasing furnace temperature, modifying the powder to reduce particle size or increase resistivity, or thermally isolating the specimen such that thermal conduction losses are minimized.

5. References

1. Cologna M, Rashkova B, Raj R. Flash sintering of nanograin zirconia in <5 s at 850 °C. J Am Ceram Soc. 2010;93(11):3556–3559.
2. Munir ZA, Quach DV. Electric current activation of sintering: a review of the pulsed electric current sintering process. J Am Ceram Soc. 2011;94(1);1–19.
3. Yu M, Grasso S, McKinnon R, Saunders T, Reece MJ. Review of flash sintering: materials, mechanisms and modelling. Adv Appl Ceram. 2016;116(1):24–60.
4. Sakka Y, Grasso S. Pulsed electrodischarged pressure sintering and flash sintering, a review. Mater Today. 2019;16:14–24.
5. Cologna M, Francis JSC, Raj R. Field assisted and flash sintering of alumina and its relationship to conductivity and MgO-doping. J Eur Ceram Soc. 2011;31(15):2827–2837.
6. Biesuz M, Sglavo VM. Flash sintering of ceramics. J Eur Ceram Soc. 2019;39(2):115–143.
7. Todd RI. Flash sintering of ceramics: a short review. Proceedings of the Advanced Ceramics and Applications Conference; 2014; Belgrade, Serbia. Amsterdam (The Netherlands): Atlantis Press; c2014. p. 1–12.
8. Todd RI, Zapata-Solvas E, Bonilla RS, Sneddon T, Wilshaw PR. Electrical characteristics of flash sintering: thermal runaway of joule heating. J Eur Ceram Soc. 2015;35(6):1865–1877.
9. Zhang Y, Jung J-I, Luo J. Thermal runaway, flash sintering and asymmetrical microstructural development of ZnO and ZnO–Bi_2O_3 under direct currents. Acta Materialia. 2015;94:87–100.
10. Charalambous H. Investigation of the mechanisms of flash sintering in oxide ceramics. [Dissertation]. [New Brunswick (NJ)]: Rutgers University; 2018.
11. Qin W, Yun J, Thron AM, van Benthem K. Temperature gradient and microstructure evolution in AC flash sintering of 3 mol% yttria-stabilized zirconia. Mater Manuf Process. 2017;32(5):549–556.
12. Steil MC, Marinha D, Aman Y, Gomes JRC, Kleitz M. From conventional AC flash-sintering of YSZ to hyper-flash and double flash. J Eur Ceram Soc. 2013;33(11):2093–2101.

13. Chaim R, Chevallier G, Weibel A, Estournès C. Grain growth during spark plasma and flash sintering of ceramic nanoparticles: a review. J Mater Sci. 2018;53(5):3087–3105.

14. Sortino E, Lebrun J-M, Sansone A, Raj R. Continuous flash sintering. J Am Ceram Soc. 2018;101(4):1432–1440.

15. Charalambous H, Jha SK, Christian KH, Lay RT, Tsakalakos T. Flash sintering using controlled current ramp. J Eur Ceram Soc. 2018;38(10)3689–3693.

16. Trombin F, Raj R. Developing processing maps for implementing flash sintering into manufacture of whiteware ceramics. Bull Am Ceram Soc. 2014;93:32–35.

17. Shomrat N, Baltianski S, Randall CA, Tsur Y. Flash sintering of potassium-niobate. J Eur Ceram Soc. 2015;35(7) 2209–2213.

18. Perez-Maqueda LA, Gil-Gonzalez E, Perejon A, Lebrun J-M, Sanchez-Jimenez PE, Raj R. Flash sintering of highly insulating nanostructured phase-pure $BiFeO_3$. J Am Ceram Soc. 2017;100(8):3365–3369.

19. Li J, Cho J, Ding J, Charalambous H, Xue S, Wang H, Phuah XL, Jian J, Wang X, Ophus C, et al. Nanoscale stacking fault–assisted room temperature plasticity in flash-sintered TiO_2. Sci Adv. 2019;5(9):eaaw5519.

20. Li YQ, Qiu T. Oxidation behaviour of boron carbide powder. Mater Sci Eng A. 2007;444:184–191.

21. Sánchez-González J, Macías-García A, Alexandre-Franco MF, Gómez-Serrano V. Electrical conductivity of carbon blacks under compression. Carbon. 2005;43(4):741–747.

List of Symbols, Abbreviations, and Acronyms

AC	alternating current
ARL	Army Research Laboratory
B_4C	boron carbide
CCDC	US Army Combat Capabilities Development Command
COV	coefficient of variation
DC	direct current
DMM	digital multimeter
DOE	design of experiments
RMS	root mean squared
SEM	scanning electron microscopy
SiC	silicon carbide
SPS	spark-plasma sintering
TiB_2	titanium diboride
YSZ	yttria-stabilized zirconia

1 (PDF)	DEFENSE TECHNICAL INFORMATION CTR DTIC OCA
1 (PDF)	CCDC ARL FCDD RLD DCI TECH LIB
2 (PDF)	CCDC ARL FCDD RLW ME A ROSENBERGER R BRENNAN